In vitro expansion of T. gondii tachyzoites using a magnetic aggregation 3D cell culture

Ana Crisitna Gomes Nascimento
Instituto de Pesquisas Energéticas e Nucleares
Giovana Dias da Silva
Instituto de Pesquisas Energéticas e Nucleares
Leonardo Wilans Pereira de Souza Rocha
Instituto de Pesquisas Energéticas e Nucleares
Priscila de Queiroz Souza Passos
Instituto Butantan
Andrés Jimenez Galisteo Jr.
Universidade de São Paulo
Luciana Regina Meireles Jaguaribe Ekman
Universidade de São Paulo
Daniel Perez Vieira (dperezv@usp.br)
Instituto de Pesquisas Energéticas e Nucleares

Research Article

Keywords: Three-dimensional cell culture, Magnetite Nanoparticles, Magnetic cell culture, Toxoplasma gondii

Posted Date: March 15th, 2022

DOI: https://doi.org/10.21203/rs.3.rs-1439798/v1

Abstract

Toxoplasma gondii is a protozoan parasite capable of infecting a wide range of living beings, including felines that are the definitive hosts of the disease, toxoplasmosis, and livestock, birds and fish. In humans, the parasite can also be present in a latent or cystic form, the latter being able to become chronic, leading to lodging in brain, retina or muscles. Infection occurs upon consuming water or food contaminated with oocysts. The tachyzoites of RH strain have fast replication and relative difficulty of maintanence exclusively in vitro, often requiring stages of in vivo cultivation in experimental animals. Three-dimensional nanoestrutucured cell cultures can be helpful to build new forms of in vitro production with potential gains in practicality and yield. This work aimed to demonstrate the feasibility of use of three-dimensional culture of murine fibroblasts aggregated to nanoparticles as substrate for T. gondii tachyzoites with the intention of facilitating the management and in vitro replication of the parasite. Magnetic aggregation was used to produce cell spheroids, which were infected with tachyzoites of RH strain and maintained in culture. After infection spheroids were evaluated by transmission electron microscopy and fluorescence microscopy with 3D rendering of image stacks. The presence of the parasite was confirmed by PCR and the number of free parasites in culture was evaluated by flow cytometry. The three-dimensional culture model used showed sustainable production of tachyzoites within 24 hours after inoculum, showing itself as a potential surrogate for the use of animals for the maintenance of the parasite.

Introduction

Toxoplasma gondii (*T. gondii*) is a mandatory intracellular protozoan parasite that infects homeothermic animals. Its life cycle requires necessary stages in gut microenvironments of felids, leading to a seroprevalence of almost 30% in domestic cats and 60% in wild felids (Montazeri et al. 2020). The infection is also common in humans (Djurković-Djaković et al. 2019), causing seroprevalences ranging from 3-4% and 9% in South Korea and UK, to 77% and 84% in Cameroon and Madagascar, respectively (Flegr et al. 2014). The main mode of infection is by ingestion of water and food contaminated by the oocystic form of the parasite and the second mode is by the consumption of undercooked or poorly processed meat containing tissue cysts, which once in the digestive tract, can differentiate into invasive form, tachyzoites. This fast replicating form of parasite invade the host cell and lyse the cells after multiplication, releasing new parasites able to invade and infect other surrounding cells. Parasites can persist for the entire life of the host in a latent form encysted in cells in tisues where the immune response is not proeminent, such as muscle, neural and retinal cells (Desmettre 2020). To date, there are no described human-to-human transmission routes, except in cases of congenital transmission and organ transplantation (Zhou et al. 2021). Infection of foetuses during pregnancy can lead to a set of symptoms, ultimately to aborption. In pregnant women, seric IgM and IgG titers were found to be detectable in 2 and 30%, respctively, showing that are a relevant portion of foetuses that can be affected by congenital toxoplasmosis.

Chronic infection of *T. gondii* is studied using rodent models, cell culture and clinical data, but there are still gaps with lack of understanding. For example, genes that control parasite development, or the mechanisms of immunity of the infected host and the long-term effects of infection, are groups of biological entities not yet fully elucidated and that require further studies. Research still in development relates diseases to toxoplasmosis such as eye diseases, inflammation of the central nervous system (CNS) and recently Alzheimer's disease (Zhao et al. 2020; Nayeri et al. 2021). The cases of spontaneous abortio due to *Toxoplasma gondii* infections have been the focus of attention in the clinical area, demonstrating the need for improvement in research (Ahmed et al. 2020). Researchers working with *T. gondii* need continuous inoculations in animals to proper carry out *in vitro* experiments. In the usual reproduction of the parasite, the inoculum of tachyzoites is used in rodent models. After reproduction of the parasite *in vivo*, the animals are euthanized and the tachyzoites can be collected by intraperitoneal successive washing (Portes et al. 2017). However, animal models are becoming increasingly expensive and can carry a number of complicating factors, such as high execution time and cost, in addition to providing little experimental precision in individual infections (Betancourt et al. 2019).

There are numerous techniques for cultivating *T. gondii* in cell monolayers (2D) *in vitro*, which help to reduce the use of animals, but one of the main main problem of continuous two-dimensional monolayer culture of toxoplasma *in vitro* is the permanent loss of infectivity of tachyzoites (Harmer et al. 1996). Some 3D cell culture techniques are being designed trying to to mimic the morphological and functional characteristics of cells and tissues *in vivo* in an attempt to provide a relevant physiological model to investigate parasite-host interactions (Betancourt et al. 2019; Luu et al. 2019; Hares et al. 2021; Holthaus et al. 2021). The altered morphology of cells grown in 2D cultures as flat monolayers can affect the morphology of the parasite (Firdaus et al. 2020), as a result of the mechanical forces acting on the infected cell and the hydrostatic pressure of the culture medium. Infection by *Toxoplasma gondii* based on 2D cell cultures is not ideal as it does not have the main conditions of *in vivo* infections, due to the presence of artificial pressures and tensions, which can alter infectious processes that depend on spatiality, for example, invasion, replication and egress. Three-dimensional cell culture (3D) models can bridge gaps between two-dimensional monolayer (2D) cultures and animal models (Danielson et al. 2018).Three-dimensional (3D) cell culture *in vitro* can simulate a tissue microenvironment *in vivo* to some extent, thus porviding fundamental information on cell-to-cell interaction. These data are being used in the understanding of tumor characteristics, metabolic profile, stem cell research and pharmacological discoveries. Cells with paramagnetic nanoparticles, when under the influence of magnetic levitation, are able to form spheroids. This proposed 3D cell culture methodology has the potential to provide alternative ways to study organ behavior through organoid construction (Jensen and Teng 2020). Paramagnetic iron oxide nanoparticles (PIONs, paramagnetic iron oxide nanoparticles) are well tolerated by tissues *in vivo and can* provide a wide range of treatments. The work used murine fibroblast spheroids generated by magnetic aggregation to stablish an alternative *in vitro* culture system to keep a provision of *T. gondii* tachyzoites.

Materials And Methods

Cell culture

NIH/3T3 mouse fibroblast (ATCC® CRL-1658) cells were cultured in 5 mL of RPMI 1640 medium, pH 7.4 (Gibco, Grand Island, USA), with 10% fetal bovine serum supplementation (Cultilab, Campinas, Brazil), 2g / L sodium bicarbonate ($NaHCO_3$, Sigma-Aldrich, Brazil) and 1% penicillin and streptomycin solution (10000 U/ 10000 µg/mL, Gibco, Carlsbad, USA) in sterile plastic cell culture flasks with 25cm^2 of culture area (Corning, Tewksbury, USA) kept in incubators in a controlled atmosphere and temperature (95% O_2, 5% CO_2, 37ºC), up to an estimated confluence of 60 to 70%. Subculture took place after depletion of the culture medium used, washing the adherent cells with 5 mL of PBS containing 5 mM EDTA (Sigma-Aldrich, Brazil). After separating the bottles, the cells were suspended in RPMI 1640 medium, prepared as described and centrifuged at 1500 rpm for 5 minutes in 15 mL conical tubes (Corning, Tewksbury, USA). Only a viable fraction, specified by incorporation of 0.4% trypan blue vital dye (Life Technologies, Carlsbad, USA) was used for subculture or experimentation.

Production of paramagnetic iron nanoparticles (PION's) for magnetic aggregation cell cultures

Magnetite nanoparticle suspensions (Fe_3O_4) were produced as described previously (Bonfim et al. 2019), but using another energy source to reduce free Fe^{2+} ions. Concentrations of iron (II) sulfate heptahydrate ($Fe_2SO_4.7H_2O$, CAS 7782-63-0) and glycine (NH_2CH_2COOH, CAS 56-40-6) were diluted in ultrapure water free of O_2 at pH 12 obtained by titration with sodium hydroxide (NaOH). Volumes of this solution were irradiated by 15kGy in the treadmill electron accelerator of the IPEN/CNEN-SP Radiation Technology Center . Black precipitates were formed, and were separated from the liquid phase by magnetic attraction and washed with ultrapure water. Subsequently, 15 mL of acetic acid were added and the solution was kept under ultrasonic agitation for 5 minutes. After this process, the acetic acid was removed and a solution of poly-lysine bromide (D-Lys-(D-Lys)n-D-Lys. xHBr) in ultrapure water at pH 7 (0.02 mg / mL) was added and kept in ultrasound for another 5 minutes. Poly-lysine carries protonable amine groups at physiological pH, which conferred a positive charge on the particles and made possible the electrostatic interaction with the cells, leading to the adsorption of the particles by the cell membranes. The final precipitates of nanoparticles were washed again with sterile ultrapure water and stored at 4 °C until the moment of application to cell culture for subsequent formation of spheroids. Magnetite formation was confirmed by X-Ray diffraction analysis (XRD) in a Orion diffractometer, model RKS-400SV-R at the Multi-user Center of the Chemistry and Environment Center (CEQMA), IPEN / CNEN-SP. Peak patterns were compared to COD database using the QualX software (Altomare et al. 2015). The crystallite size was calculated using the Debye-Scherrer equation, $D = 0.9\lambda/\beta\cos\theta$, where D is the crystal size in nm, and λ is the X-ray wavelength, β is the half-width of the peak in rad, and θ is the corresponding diffraction angle. Dilutions of nanoparticles in ultrapure water were used to evaluate the dinamic light scattering (DLS) zeta potential of the particles in a Particle Analyzer Litesizer 500 (Anton Paar) at the Center of Radiation Technology (CETER), IPEN / CNEN-SP.

Spheroids

Cells were associated with produced particles as described. The formation of spheroids consisted of exposing cell cultures to amounts of nanoparticles for 24 hours. After this period, trypsinization was performed and cells were centrifuged and resuspended with the nanoparticles in the calculated volume of culture medium for plating, 100 µL of cell suspension. Cells with nanoparticles were seeded (10^4 cells/well) in 96-well plates made of cell-repellent plastic (Cell Repellent, GreinerBioOne), and a plate with 96 magnets (Magnetic drive, GreinerBioOne) was kept below the wells in an incubator as described for cell aggregation. After obtaining cohesive spheroids, the magnet plate was removed and the plate was incubated as described .

Parasites

Toxoplasma gondii (RH strain) is routinely maintained at the Protozoology Laboratory of the Instituto de Medicina Tropical de São Paulo of the Medicine School of University of São Paulo (IMTSP-FMUSP). Tachyzoites were collected up to 96 h after intraperitoneal inoculation in Swiss mice using sterile intraperitoneal washes with cell culture medium. After 96 hours of spheroid formation, tachyzoites in medium were inoculated in a concentration of 10^4 tachyzoites / well (spheroid).

Polimerase chain reaction

Spheroids were removed from the culture plate still intact and placed in 1.5 mL microtubes together with 200 µL of PBS buffered saline solution. Each sample was subjected to genomic DNA extraction using the QIAmpMini Kit (Qiagen® GmbH) DNA kit according to the manufacturer's instructions. Samples were analyzed using NanoDrop 2000 spectrophotometer (ThermoScientific, Middlesex) and showed concentrations of 0.9 and 1.6 µg/µL. A region of the B1 gene was amplified using using the forward primer (TOXO1: 5"- GGAACTGCATCCGTTCATGAG-3") and the reverse primer (TOXO2: 5"-TCTTTAAAGGGTTCGTGGTC-3") in a Step One Plus^{TM} thermocycler (Applied Biosystems, Foster City, CA) using the following cyclic profile: initial denaturation at 94°C for 4 min, followed by 35 cycles of added denaturation at 94°C for 1 min, annealing at 62°C for 30s and an extension at 72°C for 1 min, followed by a final extension for 10 min at 72 °C. As a positive control, a total DNA extract of *T. gondii*, strain RH purified as described, was used. The amplified products were resolved on 1% agarose gels in Tris-Borate EDTA buffer (TBE) stained with ethidium bromide solution (10 μg / mL) (Veronesi et al. 2017).

Transmission electron microscopy (TEM)

Samples were stored in glass tubes containing glutaraldehyde ($C_5H_8O_2$) and processed at the laboratory of the Department of Pathology - FMUSP. The samples were centrifuged for 3 min at 6000 rpm and washed twice with 0.1M cacodylate buffer solution (pH 7.4) with sucrose (0.1M) and centrifuged again for 3 min. After centrifugation, fixed spheroids were placed in colidine buffer (osmium tetroxide), homogenized by vortexing and kept in the solution for 30 min, and were washed with cacodylate buffer and kept in alcoholic uranyl acetate (1%) for 5 min. After 5 min, samples were washed twice with 70% ethanol and then received 2,2-dimethoxypropane 5 min. The 2,2-dimethoxypropane was removed and acetone was added for 5 min. After removing the alcohol, the prepared resin 1:1 was added for 30 min.

The resin was removed again, to add the pure resin and kept for 10 min. The pellet in the tube was suspended with the aid of forceps for better penetration of the resin and left in an oven at 40°C for 10 min. The material was poured into molds in an oven at 100°C for 18 hours. After solidification of the resin, the block was ground for partial exposure of the sample. Thick slices of 0.5 µm (semifine) and 0.008 µm (MET) were performed. Staining for semifine was done with toluidine blue. A diamond blade was used to cut the material and deionized water for deposition of the cut material. The samples were stored in 3mm copper and 200µm mesh grids. These grids were dried with 11 cm filter paper after incorporation of the material. For staining, the material was left in saturated (aqueous) uranyl acetate for 15 min, then washed in deionized water and left in the solution of lead citrate and sodium citrate for 8 min. After this period, the solution was discarded in an appropriate place and the material was washed again with deionized water and stored in glasses after drying. The tomes were observed under the microscope JEM 1011 (JEOL) operated by LIM59 – Laboratory of Cell Biology, Faculty of Medicine, University of São Paulo.

Flow Cytometry

NIH/3T3 spheroids ($3x10^3$ cells) were infected $1x10^6$ by tachyzoites 72 hours after the start of magnet aggregation. At 24, 48 and 72h of inoculation, 80µL (80%) of the culture medium from each well were removed, then stained for 0.5h with 2µg / mL of Rhodamine 123 (ThermoFisher Scientific, R302), and incubated for 30 min at 37°C. After two washes with PBS, the samples were centrifuged at 10,000 rpm for 10 min and resuspended in 200 µL of PBS containing 10 µL of latex fluorescent microspheres (AccuCheck Counting Beads - Thermo-Fisher Scientific, PBC100). These spheres have an average diameter of 6µm and appear in two well-discriminated populations in FSC x SSC plots and in FL-2 (585/40 nm) by excitation at 488nm in the analysis by flow cytometry. Rhodamine 123 was excited by the equipment's laser (488nm) and its emission captured by the FL-1 channel (530/30nm). Each sample was composed by adding the volume of culture medium collected from wells in quadruplicate. The amounts of tachyzoites and beads were determined and variations in the amount of tachyzoites were expressed as the proportion between their number and the number of beads acquired (T/B ratio, or ratio). 180µL were captured per sample. The relevant events (tachyzoites and microspheres) were selected in the plots generated by the equipment using the strategy shown in Supplemental Material.

Fluorescence Microscopy (INCell Analyzer)

After extraction by peritoneal washes from infected mice, suspensions with *Toxoplasma gondii* tachyzoites were maintained in culture medium at 4°C. The parasites were concentrated by centrifugation (200 x G / 10min and then at 1000 x G / 10min, room temperature). The resulting pellet was re suspended with culture medium containing Rhodamine 123 as described. Parasite viability was determined by the trypan blue incorporation test. Spheroids of NIH/3T3 cells (5×10^3 cells per well) were formed by magnetic aggregation in repellent plastic plates as described. After 72h in culture were carefully transferred to wells of appropriate plates for evaluation by inverted microscopy (µClear®, Greiner BioOne) and received 80µL of culture medium containing 5µg / mL of Hoechst 33342 (Sigma-Aldrich, CAS

875756-97-1), which has affinity for nuclear DNA and marked nuclei of the murine cells, and were incubated for 30 minutes in an incubator. Then, each spheroid received 20µL of the tachyzoite suspension, containing $2x10^6$ viable parasites/mL. The spheroids were previewed using a Nikon Ts-100 coupled to an excitation LED module (Lumencar® Mira Light Engine 4-NII-FA) to confirm the fluorescence and subsequently evaluated by fluorescence microscopy immediately after the inoculum (0h) and 0.5, 2, 4 and 24 hours later, using the INCell Analyzer HS 2500 equipment (Cytiva). Stacks of images were generated spaced on the z axis by 4µm and one stack for each wavelength evaluated – "Green" channel evaluated the green fluorescence, emitted by tachyzoites marked by Rhodamine 123; "Blue" channel captured the fluorescence of Hoechst 33342 in the nuclei of NIH/3T3 spheroids cells and "Brightfield" channel captured the brightfield images. The equipment was adjusted to perform a 2D image acquisition every 4µm of the spheroids depth, starting from the inside to surface. A 10X magnification was used applying the 3D Convolution algorithm for further analysis of the three-dimensional structures. The stacks acquired in the "Blue" channel were analyzed using the IN Carta 1.14 package (Cytiva). The parameters were evaluated: number of NIH/3T3 cores; spheroid cross-sectional area and spheroid volume calculation. To find tachyzoites in the extracellular environment, the stacks acquired in the "Green" channel were also analyzed using the same software. For selection of only relevant events, the program parameters were adjusted to consider only events with volumes between 10 and 30μm^3, according to high resolution microscopy data of tachyzoite volumes acquired under culture conditions (Firdaus et al. 2020).

Orthogonal views of acquisitions were created from data from stacks of relevant channels and deconvolution algoritm. Three-dimensional point spreading functions (3D-PSF) for 450 (blue) and 530 (green) nanometers were estimated using PSF Generator ImageJ plugin (Kirshner et al. 2013), choosing the Born & Wolf method (Born and Wolf 1999). Stacks were finally deconvoluted using the Tikhonov-Miller method (number of iterations: 10) using the DeconvolutionLab2 plugin (Sage et al. 2017), and submitted to background correction (rolling ball radius: 50px). Events in stacks of green fluorescence were also analyzed using the "3D Object Counter" ImageJ plugin (Universitaire 2006). After initial observations, only objects with volumes between 8 and 32 voxels were included in analyses. Projections were generated using the "Extended Depth of Field" plugin (Forster et al. 2004), and results were binarized and objects were protruded in 2 dimensions by the command "Find Edges" for three consecutive iterations.

Statistical Tests and Graphical Analysis

Results were compiled in plot using Prism® 8 software (GraphPad). Statistical analysis were performed applying ANOVA test, followed by Bonferroni post-tests.

Results

Paramagnetic iron nanoparticles characterization and confirmation of crystallite composition and surface charge

Characterization of coloids produced by reduction of iron ions beam electron beam irradiation is shown in Figure 1.

The analysis software attributed distinct peaks, which could be found as characteristics of a monoclinic structure compatible with magnetite (Fe_3O_4) as depicted in peaks and planes shown in Figure 1A. Using Scherrer's calculations, it was found that crystallites formed upon electron beam irradiation had mean size of 57.98±2.509nm (Mean±SEM) (inset). Mean values of zeta potential (B) and hydrodynamic size (C) of nanoparticles coated with poly(L)Lysine chains in ultrapure water were 40.20±1.85mV and 147.50±1.6nm, respectively.

Presence of parasite DNA in spheroids assessed by PCR

Amplified DNA fragments obtained as described were subjected to electrophoresis in a TBE/agarose gel (1%). Resolved fragments are shown in Figure 2.

The bands with hypersignal in the region of interest of 286 bp are positive for the presence of the B1 gene of the parasite *Toxoplasma gondii* (RH). Samples 1 and 5 refer to parasite DNA presence in spheroids infected after 24h and 72h respectively, confirming the interaction of the parasites with the cells and the presence of parasite DNA at least until 72h after infection.

Morphological findings in image acquisitions by TEM showed evidence of intracellular tachyzoites.

NIH/3T3 spheroids infected with *T gondii* tachyzoites were visualized by TEM, and showed some peculiar findings shown in Figure 3. Cells with well-defined cytoplasm and nucleus were observed. Aggregates of iron oxide nanoparticles internalized in intracellular vacuolar structures were also clearly found. The cells of this lineage had a morphology compatible with the findings in the literature (Denardin et al. 2017; Wissel et al. 2018). It was also possible to observe the presence of electron-dense intracellular aggregates, related to the intracellular accumulation of magnetite nanoparticles.

Structures with a morphology compatible with that of intracellular tachyzoites are shown in Figure 4, and the appearance is quite comparable with other findings in works by other groups (Dubey and Lindsay 1998; Tomavo et al. 2013; Zeng et al. 2013; Seeber and Steinfelder 2016). It was also possible to observe parasite structures such as apical complex and parasitophorous vacuoles (B, D and F), as well as a coronal structure identified as the parasite's conoid. The findings present a multilamellar, intracellular structure, with electron-dense aggregations in its interior, suggesting the morphology of vacuoles with single tachyzoites transversally cut. The orientation of the tomes does not favor the display of intracellular structures of what are supposed to be tachyzoites, but there is at least one impact reference in the literature showing similar findings and in the same slice orientation (Ferguson and Dubremetz 2013). Findings in G and H were classified as tachyzoites associated with the cytoplasmic membrane of cells in cross-section, correlating the morphology found with other findings in the literature (Duarte et al. 2021; Nishi et al. 2021; Liu et al. 2021). It was possible to observe the nuclei of the parasites and structures with morphology related to that of the rhoptries.

Tachyzoites were able to reproduce in experimental conditions as assessed by flow cytometry.

Tachyzoite populations found by flow cytometry are shown in Figure 5. Tachyzoites took up Rhodamine 123 satisfactorily, allowing the discrimination of positive and negative populations. Bead populations were also easily discriminated by the fluorescence captured by FL-2.

Amounts of tachyzoites, beads and the proportions between two populations acquired in the experiments are shown in Figure 6.

The amounts of tachyzoites, beads and the T/B ratio were compared by one-way analysis of variance and Bonferroni post-test. A statistically significant increase in the amount of tachyzoites over the duration of the experiment was found; its population jumps more than 9 times in 72 hours of incubation, and such difference in relation to the beginning of the experiment (0h) is statistically significant in a very expressive way ($p < 0.0001$). Only little variations in amount of beads were found across samples, with a coefficient of variation between samples of 11.37%. Thus, they were used as a calculation baseline (or as quantification calibrators) of relative amounts of tachyzoites. However, no statistically significant differences were found between calculated T/B values.

Tachyzoites were found in peripheral zone of the spheroids, as detected by fluorescence microscopy analysis, and infection correlates with increases in the volume of tachyzoites and NIH/3T3 cell nuclei.

Tachyzoites from freshly stained Rhodamine 123 intraperitoneal washes were used as inoculum in spheroids of Hoechst 33242 stained NIH/3T3 cells. The appearance of the microscopic preparations is shown in Figure 7.

The mitochondria of tachyzoites were successfully labeled by Rhodamine 123, giving them green fluorescence, according to previous reports (Tanabe 1985; de Melo et al. 1992; Souza and Belfort Jr. 2014). The figure shows fusiform objects with smaller size in relation to the cells, compatible with the sightings of *T. gondii* tachyzoites in culture. There were also artifacts with dimensions larger than those found in the tachyzoites, and their occurrence was related to the presence of material of murine origin in the suspension used, since mice were used to reproduce the strain in the step prior to the *in vitro* inoculum. Such spurious events appeared much less frequent from the culture after about 24 hours after inoculum, and there was no evidence of interference in the experiment, although their presence was undesirable.

After confirmation of tachyzoite labeling, the spheroids were observed in the INCell Analyzer 2500HS equipment. Typical appearance NIH/3T3 cell nuclei and tachyzoites 24 hours after inoculum is shown in Figure 8.

The occurrence of tachyzoites was discreetly perceived due to the poor penetration of light in extense bodies, limiting the resolution of acquisitons. However, it was possible to infer the occurrence of tachyzoites preferentially in peripheral strata of spheroids, composing, in a way, a specific kind of epifauna having the spheroid as a physical substrate.

Image stacks of NIH/3T3 spheroid acquired 0.5, 2, 4 and 24 hours after inoculation with *T. gondii* tachyzoites were analyzed. The volume of found tachyzoites, NIH/3T3 nuclei, spheroids and the number of tachyzoites were evaluated by INCarta software and are shown in Figure 9

The mean volume of tachyzoites appeared to be increased after 2, 4 or 24 hour after inoculum; a similar response could be observed in nuclei from NIH/3T3 only after 24 hours after inoculum, and no differences were found in spheroid volumes or in the numbers of epifaunal tachyzoites during 24 hours of experiment.

Orthogonal projections of some findings of spheroid after 24 hours of infection are in Figure 10.

Discussion

Particles such as those used in this work were previously identified in the extracellular medium, forming aggregates adsorbed on cytoplasmic membranes (Bonfim et al. 2019), but their intracellular occurrence was detected in other studies (Ho et al. 2012; Calero et al. 2014; Mattix et al. 2014; Mazuel et al. 2016; Feng et al. 2018). The entry of iron oxide nanoparticles into cells occurs through several phenomena, however, given the specific coating of the nanoparticles used in this study with long poly(L)lysine chains, giving them cationic potential, it is likely that their internalization occurred through interaction with surface proteoglycans, such as heparin and heparan sulfate and chondroitin sulfates (Rueda-Gensini et al. 2020). Its presence stimulates the aggregation of particles, which in turn stimulates the endocytosis of such aggregates (Poon and Gariépy 2007; Siow et al. 2018). Still regarding the surface charge of the particles, there is evidence reporting that the internalization of positively charged iron oxide nanoparticles is concentrated in the cortical layers of the spheroids, apparently by electrostatic interactions with extracellular matrix proteins (Tchoryk et al. 2019) .

After internalization, the parasite is surrounded by a parasitophorous vacuole (Ferguson 2009), a multilamellar sac-like structure composed of both parasite and host components (Coppens et al. 2006). After the development of endodyogenic reproduction processes, about eight tachyzoites can be formed, which will have a rosette appearance (Boothroyd and Dubremetz 2008). The work failed to detect such structures, but as reported by others (Ferguson and Dubremetz 2013), the findings have relative resemblance to newly formed parasitophorous vacuoles, hence the presence of a single tachyzoite.

Structures with a morphology compatible with that of intracellular tachyzoites were found, and the appearance is quite comparable with that of other findings in works by other groups (Dubey et al. 1998; Tomavo et al. 2013; Zeng et al. 2013; Seeber and Steinfelder 2016). It was even possible to observe parasite structures such as apical complex and parasitophorous vacuoles, as well as a coronal structure identified as the parasite's conoid. Findings with an appearance close to the presence of parasitophorous vacuoles were detected, and were classified as tachyzoites associated with the cytoplasmic membrane of the cells in cross-section, correlating the morphology found with other findings in the literature (Duarte et al. 2021; Nishi et al. 2021; Liu et al. 2021). It was possible to observe the nuclei of the parasites and rhoptries.

The detection of fluorescence of rhodamines uptaken by *T. gondii* is a well described technique (Tanabe 1985; de Melo et al. 1992; De-Souza et al. 1998; Melo et al. 2000), more usually in fluorescence microscopy experiments. There is one report of using direct detection of Rhodamine 123 for assessment of bacterial growth on culture (Davey et al. 1993), but no evidence was found of using of this technique in protozoal *in vitro* multiplcation, as employed by this work.

Preliminary tests showed that there was a homogeneous distribution of live and non-viable cells in the produced spheroids, so that an effect of predominantly cortical cell viability and internalized mortality in the spheroids was not observed, which is a common and observable effect in this in vitro culture system (Khaitan et al. 2006; Sato et al. 2015; Hari et al. 2019; Lewin et al. 2020; Štampar et al. 2020). Thus, the occurrence of an outer cell layer with an accelerated proliferation rate could not explain the apparent preference of tachyzoites for lodging in the periphery of the spheroids. It is possible to associate this behavior with the simple availability of gases and nutrients, which is higher on the surface, and in the concentrations of excreta, which are higher inside the spheroids (Barisam et al. 2018; Gomes et al. 2018; Štampar et al. 2020; Han et al. 2021), thus attracting tachyzoites to less aggressive environments. These parasites forms have positive chemotaxis to several amino acids, cholesterol, polyamines and iron (Laliberté and Carruthers 2008), elements present in the culture medium and, therefore, in greater amounts in the extracellular medium, which may have kept the tachyzoites in the epifauna. The molecular mechanisms of tachyzoite chemotaxis are extensive, described in other works (Laliberté and Carruthers 2008; Blume and Seeber 2018) and go beyond the scope of this work, not having been addressed in depth.

According to recent literature (Firdaus et al. 2020), increase in mammalian cell volume is expected after *in vitro* infection by *T. gondii* tachyzoites. The present study could detect such diference in the volume of NIH/3T3 cell nuclei 24 hours after infection, during which theoretically more than one parasite division cycle may be completed (Radke et al. 2001). Parasite GRA16 protein can be translocated to the nuclei of host cells, leading to changes in the gene expression profile and transcription levels (Bougdour et al. 2013). Furthermore, *T. gondii* infection induces cell cycle arrest between S phase and G2/M phase, inducing an increase in the number of multiploid cell, which could at least partially explain the increase in nuclear volume (Velásquez et al. 2019). The reduction of the median parasite volume in the conditions of this work could not be explained by the present experiments or through data collected elsewhere. The total volume of spheroids did not change during the experiment, nor did the number of tachyzoites in the epifauna. However, flow cytometry data showed a very significant increase in the number of tachyzoites collected in the culture medium, corroborating to a some extent the free-swimming behavior of the parasite. Further experiments could be directed to show whether epifauna tachyzoites are parasites that are either about to invade a host cell or have just broken through the membrane and released to medium.

The work is one of the first to report cultivation of *T. gondii* in a three-dimensional culture model (after (Danielson et al. 2018)) and so far the only one to report cultivation in spheroids, and not only in cells dispersed in extracellular matrix. The data showed that it is possible to cultivate tachyzoites in such models, and provides experimental basis for refinements that can elucidate parasite preferences for

specific cell types, effect of pH and nutrient amounts on infection, depth of tissues that would be subject to invasion, and even a possible model for the cultivation of bradyzoites and their cysts, whose techniques still need improvement (Christiansen et al. 2021). In addition, the technique made it possible to open a horizon of *in vitro* cultivation that could aim to eliminate the use of animals to maintain the strains, with laboratories simply collecting the culture medium with parasites and using the suspensions to reinfect new spheroids in culture. .

Declarations

Author Contributions Statement

1. Ana Cristina Gomes Nascimento - Most of experimental work

2. Giovana Dias da Silva and 3. Giovana Dias da Silva - Technical support of experiments

4. Priscila de Queiroz Souza Passos - Production of iron nanoparticles

5. Andrés Jimenez Galisteo Jr. and 6. Luciana Regina Meireles Jaguaribe Ekman - Parasite cultivation and support

7. Daniel Perez Vieira - Experiment design, analysis and scientific writing

Statements and Declarations:

Authors declare no conflicts of interest

References

1. Ahmed M, Sood A, Gupta J (2020) Toxoplasmosis in pregnancy. Eur J Obstet Gynecol Reprod Biol 255:44–50. https://doi.org/10.1016/j.ejogrb.2020.10.003
2. Altomare A, Corriero N, Cuocci C, et al (2015) QUALX2.0: A qualitative phase analysis software using the freely available database POW-COD. J Appl Crystallogr 48:598–603. https://doi.org/10.1107/S1600576715002319
3. Barisam M, Saidi MS, Kashaninejad N, Nguyen NT (2018) Prediction of necrotic core and hypoxic zone of multicellular spheroids in a microbioreactor with a U-shaped barrier. Micromachines 9:1–19. https://doi.org/10.3390/mi9030094
4. Betancourt ED, Hamid B, Fabian BT, et al (2019) From entry to early dissemination-Toxoplasma gondii'sInitial Encounter with Its Host. Front Cell Infect Microbiol 9:1–9. https://doi.org/10.3389/fcimb.2019.00046
5. Blume M, Seeber F (2018) Metabolic interactions between toxoplasma gondii and its host [version 1; peer review: 2 approved]. F1000Research 7:1–10. https://doi.org/10.12688/F1000RESEARCH.16021.1

6. Bonfim L, Passos PQS, Gonçalves KO, et al (2019) Microwave-mediated synthesis of iron-oxide nanoparticles for use in magnetic levitation cell cultures. Appl Nanosci 9:1707–1717. https://doi.org/10.1007/s13204-019-00962-1
7. Boothroyd JC, Dubremetz JF (2008) Kiss and spit: The dual roles of Toxoplasma rhoptries. Nat Rev Microbiol 6:79–88. https://doi.org/10.1038/nrmicro1800
8. Born M, Wolf E (1999) Principles of optics : electromagnetic theory of propagation, interference and diffraction of light, 7th edn. Cambridge University Press
9. Bougdour A, Durandau E, Brenier-Pinchart MP, et al (2013) Host cell subversion by Toxoplasma GRA16, an exported dense granule protein that targets the host cell nucleus and alters gene expression. Cell Host Microbe 13:489–500. https://doi.org/10.1016/j.chom.2013.03.002
10. Calero M, Gutiérrez L, Salas G, et al (2014) Efficient and safe internalization of magnetic iron oxide nanoparticles: Two fundamental requirements for biomedical applications. Nanomedicine Nanotechnology, Biol Med 10:733–743. https://doi.org/10.1016/j.nano.2013.11.010
11. Christiansen C, Maus D, Melerowicz F, et al (2021) A Novel in vitro Model for Mature Toxoplasma gondii Bradyzoites Reveals their Metabolome and a Diminished Role of the Mitochondrial Tricarboxylic Acid Cycle. bioRxiv 2021.01.15.426845
12. Coppens I, Dunn JD, Romano JD, et al (2006) Toxoplasma gondii Sequesters Lysosomes from Mammalian Hosts in the Vacuolar Space. Cell 125:261–274. https://doi.org/10.1016/j.cell.2006.01.056
13. Danielson JJ, Perez N, Romano JD, Coppens I (2018) Modelling Toxoplasma gondii infection in a 3D cell culture system In Vitro: Comparison with infection in 2D cell monolayers. PLoS One 13:1–13. https://doi.org/10.1371/journal.pone.0208558
14. Davey HM, Kaprelyants AS, Kell DB (1993) Flow Cytometric Analysis, Using Rhodamine 123, of Micrococcus luteus at Low Growth Rate in Chemostat Culture. Flow Cytom Microbiol 83–93. https://doi.org/10.1007/978-1-4471-2017-9_6
15. De-Souza W, De-Carvalho TU, De-Melo ET, et al (1998) The use of confocal laser scanning microscopy to analyze the process of parasitic protozoon-host cell interaction. Brazilian J Med Biol Res 31:1459–1470. https://doi.org/10.1590/S0100-879X1998001100015
16. de Melo EJT, de Carvalho TU, de Souza W (1992) Penetration of Toxoplasma gondii into Host Cells Induces Changes in the Distribution of the Mitochondria and the Endoplasmic Reticulum. Cell Struct Funct 17:311–317. https://doi.org/10.1247/csf.17.311
17. Denardin CC, Martins LAM, Parisi MM, et al (2017) Autophagy induced by purple pitanga (Eugenia uniflora L.) extract triggered a cooperative effect on inducing the hepatic stellate cell death. Cell Biol Toxicol 33:197–206. https://doi.org/10.1007/s10565-016-9366-5
18. Desmettre T (2020) Toxoplasmosis and behavioural changes. J Fr Ophtalmol 43:e89–e93. https://doi.org/10.1016/j.jfo.2020.01.001
19. Djurković-Djaković O, Dupouy-Camet J, Van der Giessen J, Dubey JP (2019) Toxoplasmosis: Overview from a One Health perspective. Food Waterborne Parasitol 15:12–15.

https://doi.org/10.1016/j.fawpar.2019.e00054

20. Duarte AGP, Carvalho GOAM de, Franzen AJ, et al (2021) Anti-Toxoplasma Gondii Effect of Metalocomplex Compounds N0414 and N5814 / Efeito Anti-Toxoplasma Gondii Do Composto Metalocomplexo N0414 E N5814. Brazilian J Dev 7:16541–16555. https://doi.org/10.34117/bjdv7n2-330
21. Dubey JP, Lindsay DS (1998) Structures of Toxoplasma gondii Tachyzoites , Bradyzoites , and Sporozoites and Biology and Development of Tissue Cysts †. 11:267–299
22. Dubey JP, Lindsay DS, Speer CA (1998) Structures of Toxoplasma gondii tachyzoites, bradyzoites, and sporozoites and biology and development of tissue cysts. Clin Microbiol Rev 11:267–299. https://doi.org/10.1128/cmr.11.2.267
23. Feng Q, Liu Y, Huang J, et al (2018) Uptake, distribution, clearance, and toxicity of iron oxide nanoparticles with different sizes and coatings. Sci Rep 8:1–13. https://doi.org/10.1038/s41598-018-19628-z
24. Ferguson DJP (2009) Toxoplasma gondii: 1908-2008, homage to Nicolle, Manceaux and Splendore. Mem Inst Oswaldo Cruz 104:133–148. https://doi.org/10.1590/S0074-02762009000200003
25. Ferguson DJP, Dubremetz JF (2013) The Ultrastructure of Toxoplasma gondii, Second Edi. Elsevier
26. Firdaus ER, Park JH, Lee SK, et al (2020) 3D morphological and biophysical changes in a single tachyzoite and its infected cells using three-dimensional quantitative phase imaging. J Biophotonics 13:. https://doi.org/10.1002/jbio.202000055
27. Flegr J, Prandota J, Sovičková M, Israili ZH (2014) Toxoplasmosis - A global threat. Correlation of latent toxoplasmosis with specific disease burden in a set of 88 countries. PLoS One 9:. https://doi.org/10.1371/journal.pone.0090203
28. Forster B, Van De Ville D, Berent J, et al (2004) Complex wavelets for extended depth-of-field: A new method for the fusion of multichannel microscopy images. Microsc Res Tech 65:33–42. https://doi.org/10.1002/jemt.20092
29. Gomes A, Defaux M, Lemee RM, et al (2018) Reversible growth arrest of 3D tumor spheroids stored in oxygen absorber-induced anoxia. Oncol Lett 15:2006–2009. https://doi.org/10.3892/ol.2017.7465
30. Han SJ, Kwon S, Kim KS (2021) Challenges of applying multicellular tumor spheroids in preclinical phase. Cancer Cell Int 21:1–19. https://doi.org/10.1186/s12935-021-01853-8
31. Hares MF, Tiffney EA, Johnston LJ, et al (2021) Stem cell-derived enteroid cultures as a tool for dissecting host-parasite interactions in the small intestinal epithelium
32. Hari N, Patel P, Ross J, et al (2019) Optical coherence tomography complements confocal microscopy for investigation of multicellular tumour spheroids. Sci Rep 9:1–11. https://doi.org/10.1038/s41598-019-47000-2
33. Harmer C, Aspöck H, Hassl A (1996) Toxoplasma gondii in vitro cultivation: easy handling long-term propagation. J Microbiol Methods 27:221–223. https://doi.org/10.1016/S0167-7012(96)00952-9

34. Ho DN, Kohler N, Sigdel A, et al (2012) Penetration of endothelial cell coated multicellular tumor spheroids by iron oxide nanoparticles. Theranostics 2:66–75. https://doi.org/10.7150/thno.3568
35. Holthaus D, Delgado-Betancourt E, Aebischer T, et al (2021) Harmonization of Protocols for Multi-Species Organoid Platforms to Study the Intestinal Biology of Toxoplasma gondii and Other Protozoan Infections. Front Cell Infect Microbiol 10:1–18. https://doi.org/10.3389/fcimb.2020.610368
36. Jensen C, Teng Y (2020) Is It Time to Start Transitioning From 2D to 3D Cell Culture? Front Mol Biosci 7:1–15. https://doi.org/10.3389/fmolb.2020.00033
37. Khaitan D, Chandna S, Arya MB, Dwarakanath BS (2006) Establishment and characterization of multicellular spheroids from a human glioma cell line; implications for tumor therapy. J Transl Med 4:1–13. https://doi.org/10.1186/1479-5876-4-12
38. Kirshner H, Aguet F, Sage D, Unser M (2013) 3-D PSF fitting for fluorescence microscopy: Implementation and localization application. J Microsc 249:13–25. https://doi.org/10.1111/j.1365-2818.2012.03675.x
39. Laliberté J, Carruthers VB (2008) Host cell manipulation by the human pathogen Toxoplasma gondii. Cell Mol Life Sci 65:1900–1915. https://doi.org/10.1007/s00018-008-7556-x
40. Lewin TD, Maini PK, Moros EG, et al (2020) A three phase model to investigate the effects of dead material on the growth of avascular tumours. Math Model Nat Phenom 15:22. https://doi.org/10.1051/mmnp/2019039
41. Liu Y, Tang Y, Tang X, et al (2021) Anti-Toxoplasma gondii Effects of a Novel Spider Peptide XYP1 In Vitro and In Vivo. Biomedicines 9:934. https://doi.org/10.3390/biomedicines9080934
42. Luu L, Johnston LJ, Derricott H, et al (2019) An open-format enteroid culture system for interrogation of interactions between Toxoplasma gondii and the intestinal epithelium. Front Cell Infect Microbiol 9:1–19. https://doi.org/10.3389/fcimb.2019.00300
43. Mattix B, Olsen TR, Gu Y, et al (2014) Biological magnetic cellular spheroids as building blocks for tissue engineering. Acta Biomater 10:623–629. https://doi.org/10.1016/j.actbio.2013.10.021
44. Mazuel F, Espinosa A, Luciani N, et al (2016) Massive Intracellular Biodegradation of Iron Oxide Nanoparticles Evidenced Magnetically at Single-Endosome and Tissue Levels. ACS Nano 10:7627–7638. https://doi.org/10.1021/acsnano.6b02876
45. Melo EJL, Attias M, De Souza W (2000) The single mitochondrion of tachyzoites of Toxoplasma gondii. J Struct Biol 130:27–33. https://doi.org/10.1006/jsbi.2000.4228
46. Montazeri M, Mikaeili Galeh T, Moosazadeh M, et al (2020) The global serological prevalence of Toxoplasma gondii in felids during the last five decades (1967-2017): A systematic review and meta-analysis. Parasites and Vectors 13:1–10. https://doi.org/10.1186/s13071-020-3954-1
47. Nayeri T, Sarvi S, Sharif M, Daryani A (2021) Toxoplasma gondii: A possible etiologic agent for Alzheimer's disease. Heliyon 7:e07151. https://doi.org/10.1016/j.heliyon.2021.e07151
48. Nishi L, Sanfelice RADS, Bortoleti BTDS, et al (2021) Moringa oleifera extract promotes apoptosis-like death in Toxoplasma gondii tachyzoites in vitro. Parasitology.

https://doi.org/10.1017/S0031182021001086

49. Poon GMK, Gariépy J (2007) Cell-surface proteoglycans as molecular portals for cationic peptide and polymer entry into cells. Biochem Soc Trans 35:788–793. https://doi.org/10.1042/BST0350788
50. Portes JA, Motta CS, Azeredo NF, et al (2017) In vitro treatment of Toxoplasma gondii with copper(II) complexes induces apoptosis-like and cellular division alterations. Vet Parasitol 245:141–152. https://doi.org/10.1016/j.vetpar.2017.04.002
51. Radke JR, Striepen B, Guerini MN, et al (2001) Defining the cell cycle for the tachyzoite stage of Toxoplasma gondii. Mol Biochem Parasitol 115:165–175. https://doi.org/10.1016/S0166-6851(01)00284-5
52. Rueda-Gensini L, Cifuentes J, Castellanos MC, et al (2020) Tailoring iron oxide nanoparticles for efficient cellular internalization and endosomal escape. Nanomaterials 10:1–56. https://doi.org/10.3390/nano10091816
53. Sage D, Donati L, Soulez F, et al (2017) DeconvolutionLab2: An open-source software for deconvolution microscopy. Methods 115:28–41. https://doi.org/10.1016/j.ymeth.2016.12.015
54. Sato K, Nagaya T, Nakamura Y, et al (2015) Near infrared photoimmunotherapy prevents lung cancer metastases in a murine model. Oncotarget 6:19747–19758. https://doi.org/10.18632/oncotarget.3850
55. Seeber F, Steinfelder S (2016) Recent advances in understanding apicomplexan parasites. F1000Research 5:1369. https://doi.org/10.12688/f1000research.7924.1
56. Siow WX, Chang YT, Babič M, et al (2018) Interaction of poly-L-lysine coating and heparan sulfate proteoglycan on magnetic nanoparticle uptake by tumor cells. Int J Nanomedicine 13:1693–1706. https://doi.org/10.2147/IJN.S156029
57. Souza W de, Belfort Jr. R (2014) Toxoplasmose & Toxoplasma gondii
58. Štampar M, Breznik B, Filipič M, Žegura B (2020) Characterization of In Vitro 3D Cell Model Developed from Human Hepatocellular Carcinoma (HepG2) Cell Line. Cells 9:2557. https://doi.org/10.3390/cells9122557
59. Tanabe K (1985) Visualization of the mitochondria of Toxoplasma gondii-infected mouse fibroblasts by the cationic permeant fluorescent dye rhodamine 123. Experientia 41:101–102. https://doi.org/10.1007/BF02005897
60. Tchoryk A, Taresco V, Argent RH, et al (2019) Penetration and uptake of nanoparticles in 3D tumor spheroids. Bioconjug Chem 30:1371–1384. https://doi.org/10.1021/acs.bioconjchem.9b00136
61. Tomavo S, Slomianny C, Meissner M, Carruthers VB (2013) Protein Trafficking through the Endosomal System Prepares Intracellular Parasites for a Home Invasion. PLoS Pathog 9:. https://doi.org/10.1371/journal.ppat.1003629
62. Universitaire C (2006) A guided tour into subcellular colocalization analysis in light. 224:213–232
63. Velásquez ZD, Conejeros I, Larrazabal C, et al (2019) Toxoplasma gondii-induced host cellular cell cycle dysregulation is linked to chromosome missegregation and cytokinesis failure in primary

endothelial host cells. Sci Rep 9:1–16. https://doi.org/10.1038/s41598-019-48961-0

64. Veronesi F, Santoro A, Milardi GL, et al (2017) Detection of Toxoplasma gondii in faeces of privately owned cats using two PCR assays targeting the B1 gene and the 529-bp repetitive element. Parasitol Res 116:1063–1069. https://doi.org/10.1007/s00436-017-5388-z
65. Wissel K, Brandes G, Pütz N, et al (2018) Platinum corrosion products from electrode contacts of human cochlear implants induce cell death in cell culture models. PLoS One 13:1–20. https://doi.org/10.1371/journal.pone.0196649
66. Zeng YB, Dong H, Han HY, et al (2013) The ultrastructural effects of sulfachloropyrazine on Toxoplasma gondii tachyzoites. Iran J Parasitol 8:73–77
67. Zhao X, Ewald SE, Zhao X, Ewald SE (2020) The molecular biology and immune control of chronic Toxoplasma gondii infection The molecular biology and immune control of chronic Toxoplasma gondii infection. 130:3370–3380
68. Zhou Z, Ortiz Lopez HIA, Pérez GE, et al (2021) Toxoplasmosis and the Heart. Curr Probl Cardiol 46:100741. https://doi.org/10.1016/j.cpcardiol.2020.100741

Figures

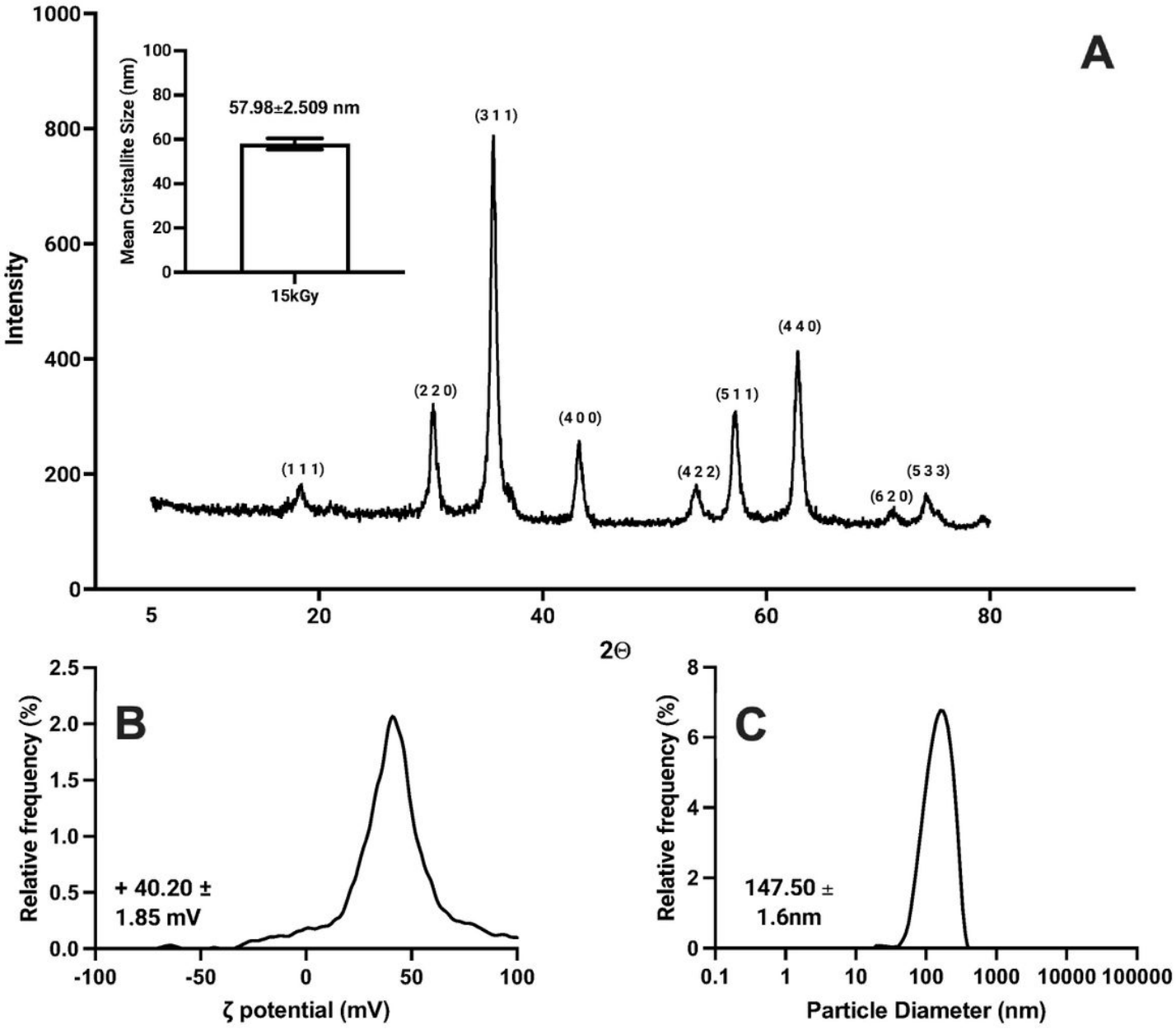

Figure 1

(A): X-ray diffraction spectrum of iron crystallites formed upon electron beam radiation (15 kGy). Inset: Mean size of crystallites, calculated using Scherrer's equation. Error bar: Stardard error of means (SEM). (B): Measurements of zeta potential (mV) of particle suspension. (C): Hydrodynamic size (nm) of the nanoparticles.

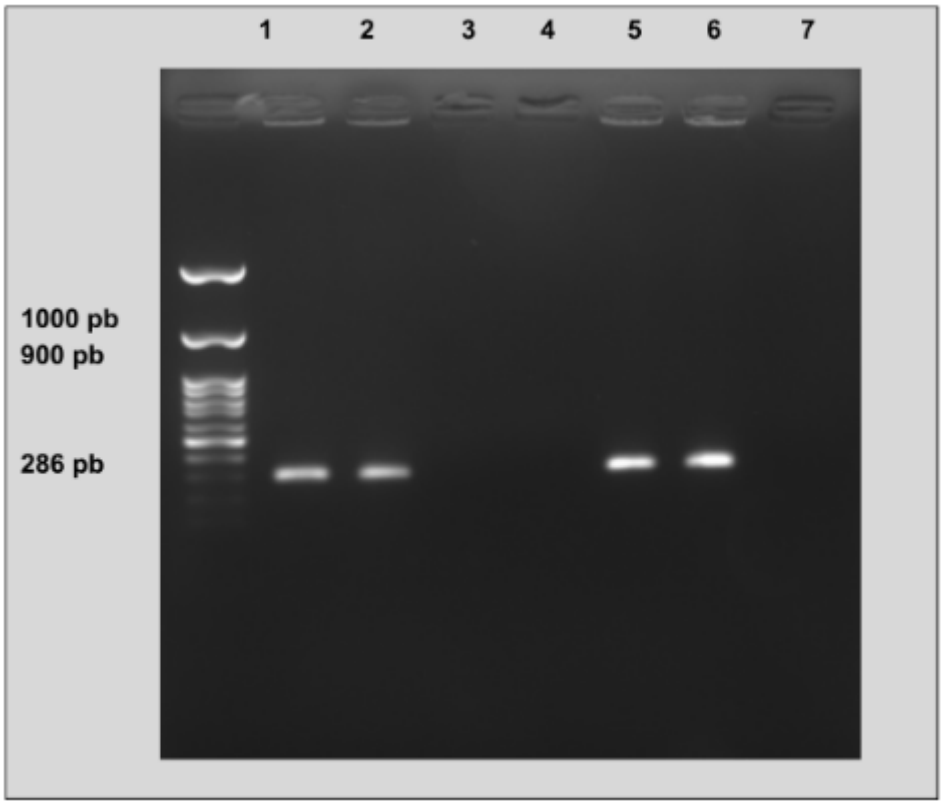

Figure 2

Agarose gel containing resolved DNA fragments after amplification. First lane: Size marker (100bp). Lane 1: DNA of spheroids infected with $1x10^4$ tachyzoites, 24 hours after inoculation; Lane 2: Parasite DNA from peritoneal wash containing $1x10^4$ tachyzoites, positive control; Lane 3: DNA of spheroid without parasites, negative control; Lane 4: Sterile H_2O, negative amplification control; Lane 5: DNA of spheroids infected with $1x10^4$ tachyzoites, 72 hours after inoculation; Lane 6: Same as Lane 2; Lane 7: same as Lane 3.

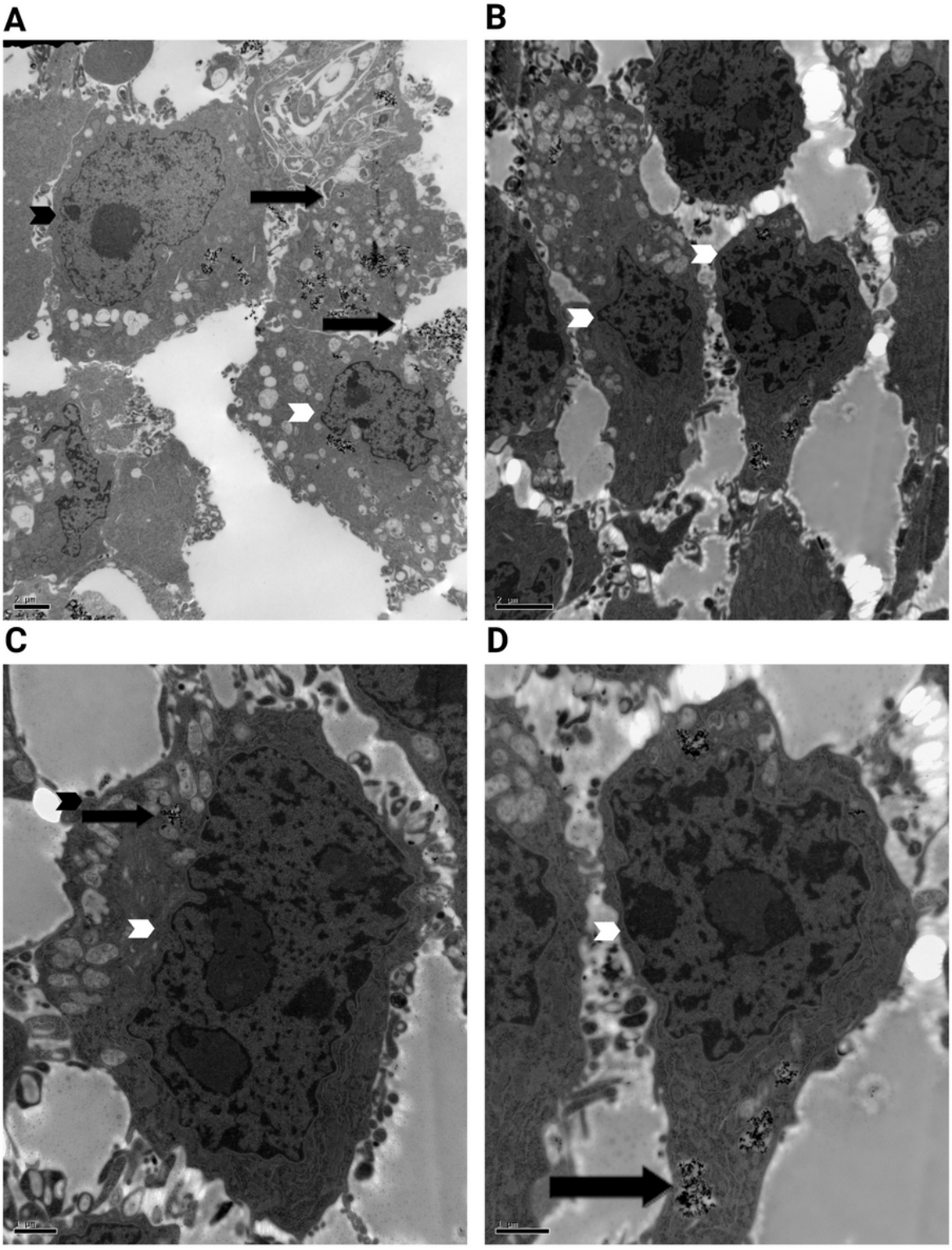

Figure 3

NIH/3T3 spheroids produced by magnetic aggregation observed by transmission electron microscopy. Magnifications: (A): 5000X; (B): 8000X; (C): 12000X; (D): 15000X. Arrows: aggregates of magnetite nanoparticles. Chevrons: cell nuclei.

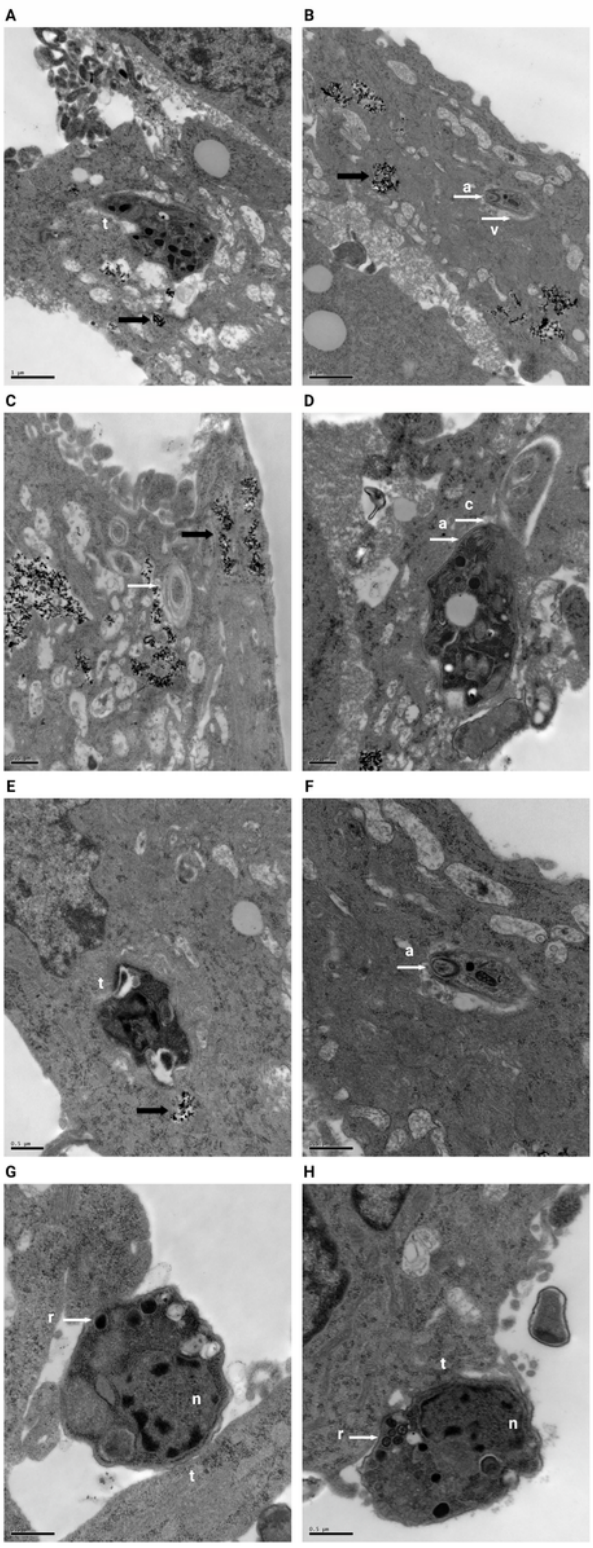

Figure 4

Ultrastructural findings observed in NIH/3T3 spheroids infected with *T. gondii* tachyzoites. Black arrows: intracellular aggregates of magnetite nanoparticles. (t): morphology compatible with that of an intracellular tachyzoite of *T.gondii*. (a): structure morphologically identified as apical tachyzoite complex. (c): structure morphologically identified as a tachyzoite conoid. (v): structure morphologically identified as a parasitophorous vacuole. (n) tachyzoite nucleus. (r): structure morphologically identified as rhoptry.

White arrows and chevrons: structure morphologically identified as a parasitophorous vacuole. Detail of the tachyzoite in (B) was visualized at higher magnification in (F). Magnifications: (A) and (B): 20000X; (C) and (D): 25000X; (E): 30000X; (F), (G) and (H): 40000X.

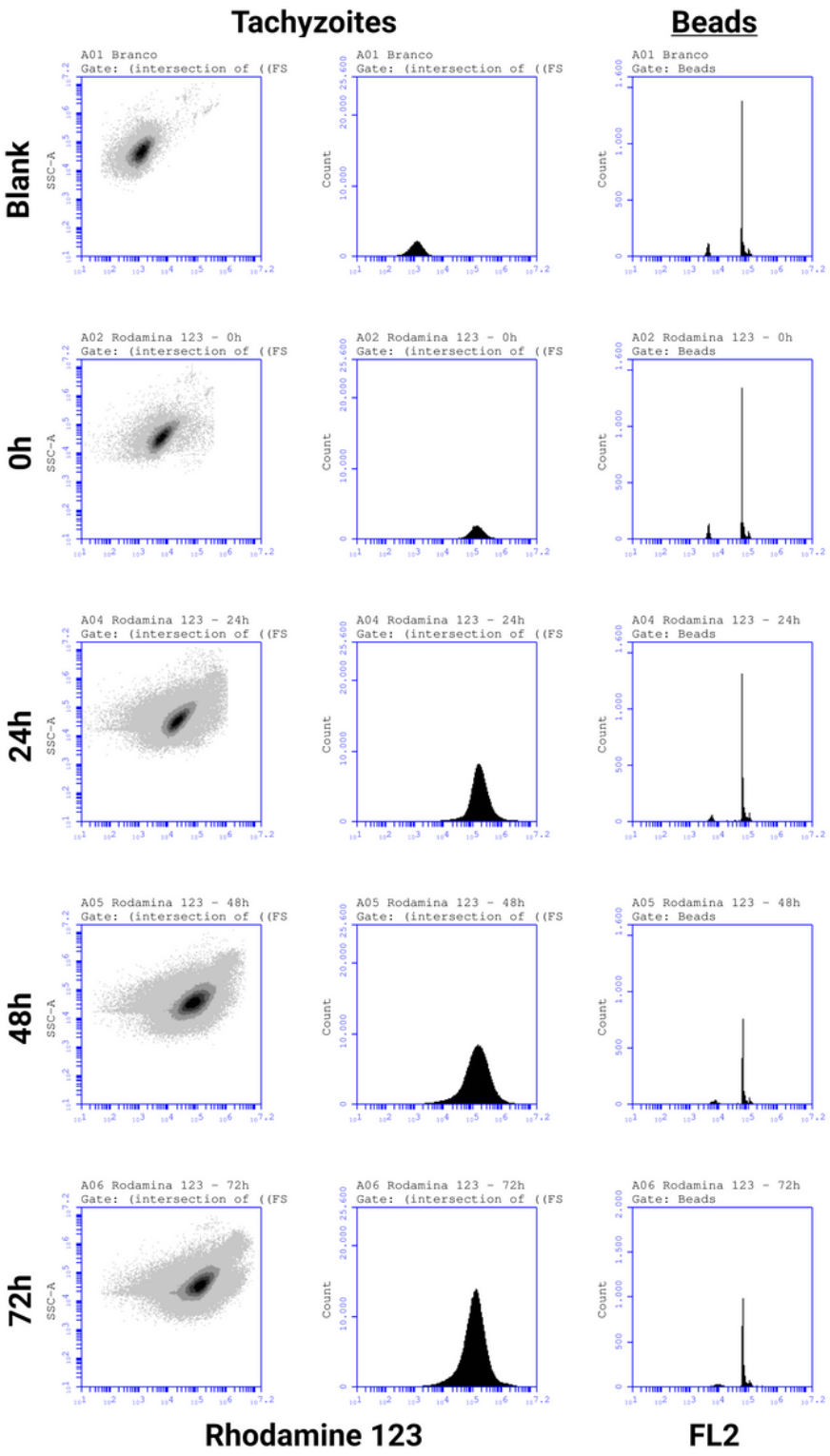

Figure 5

Populations of tachyzoites labeled with Rhodamine 123 and beads. The figure shows the unlabeled (“blank”) and labeled populations after 0, 24, 48 or 72 hours after inoculation on the spheroids. Left and middle columns: tachyzoite populations acquired and displayed in dot plots or histograms, respectively. Right column: Bead populations.

Figure 6

A – Histogram showing *T. gondii* tachyzoite populations acquired by the equipment after incubations for 0 (red), 24 (green), 48 (blue) and 72 (magenta) hours with the fibroblast spheroids. B – bead populations. C – bar graph showing the amounts of tachyzoites (white bars; left axis) and the proportion between tachyzoites and beads (T/B, gray bars, right axis). Error bars: mean of standard error. Asterisks indicate statistically significant differences in relation to the control (0h of incubation). (*): $p < 0.05$. (****): $p < 0.0001$. D – table with the values obtained in the acquisitions.

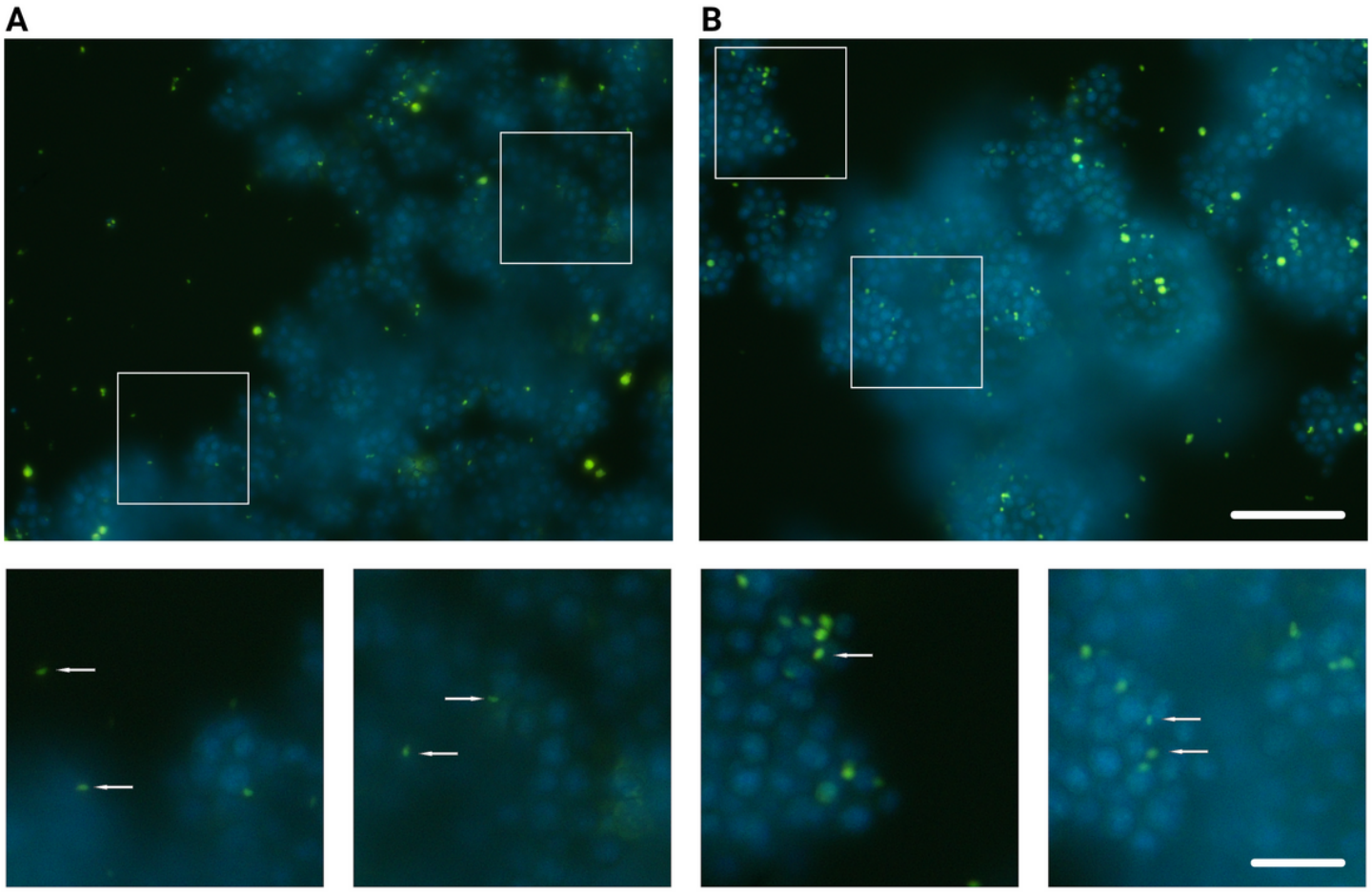

Figure 7

NIH/3T3 spheroids inoculated with T. gondii tachyzoites and evaluated by fluorescence microscopy 30 (A) or 60 minutes (B) after inoculum. Blue: Cell nuclei labeled with Hoechst 332412. Green: T. gondii tachyzoites labeled with Rhodamine 123A, highlighted by white arrows. Magnification: 10X (highlight: 24X, digital). Bars: 100µm.

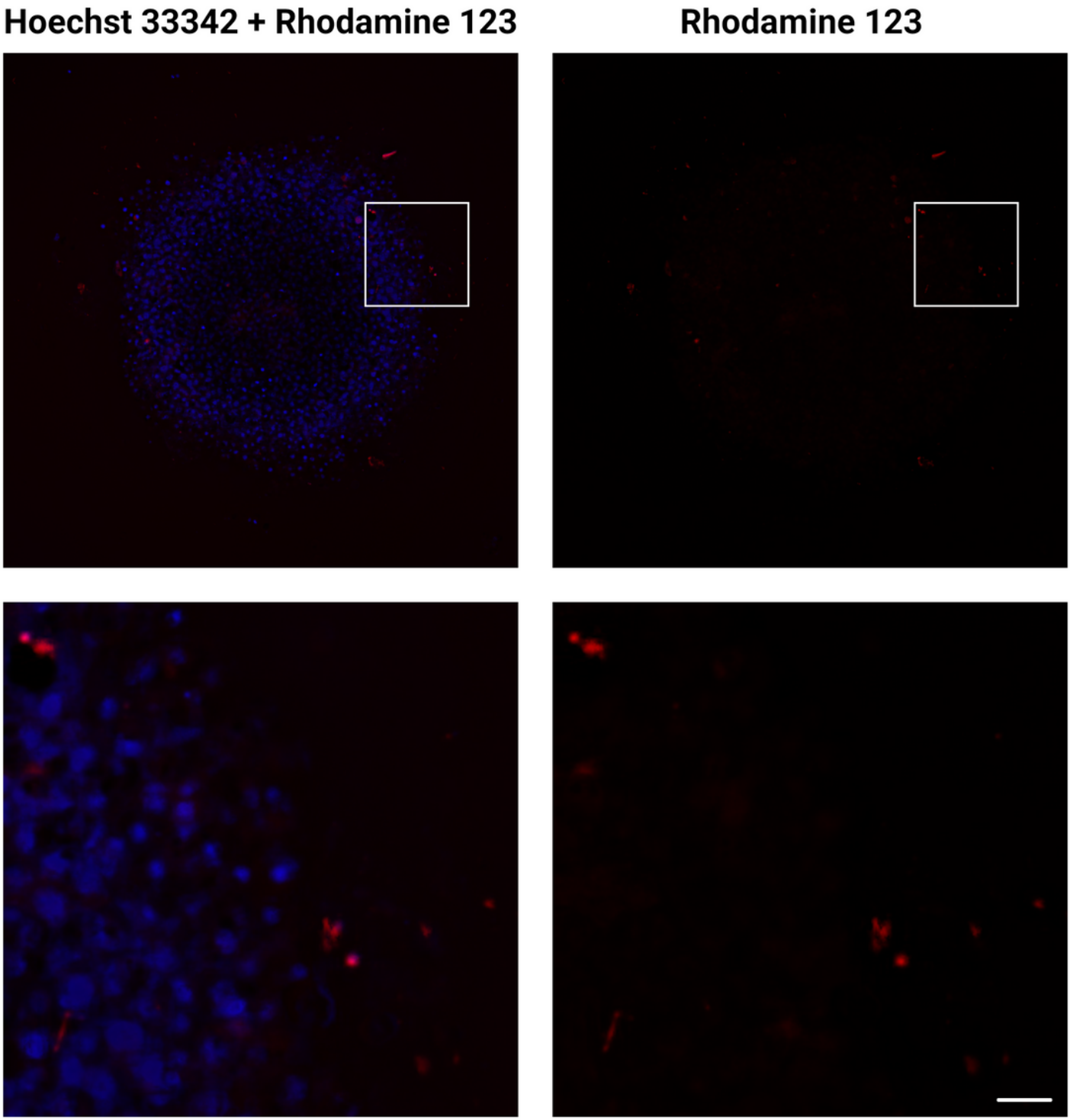

Figure 8

NIH/3T3 spheroid inoculated with *T. gondii* tachyzoites and evaluated by fluorescence microscopy 24 hours after inoculum. Blue: Cell nuclei labeled with Hoechst 332412. Red: *T. gondii* tachyzoites labeled with Rhodamine 123A (pseudocolor). Magnifications - Above: 10X; Below: 30X (digital). Bar: 33µm.

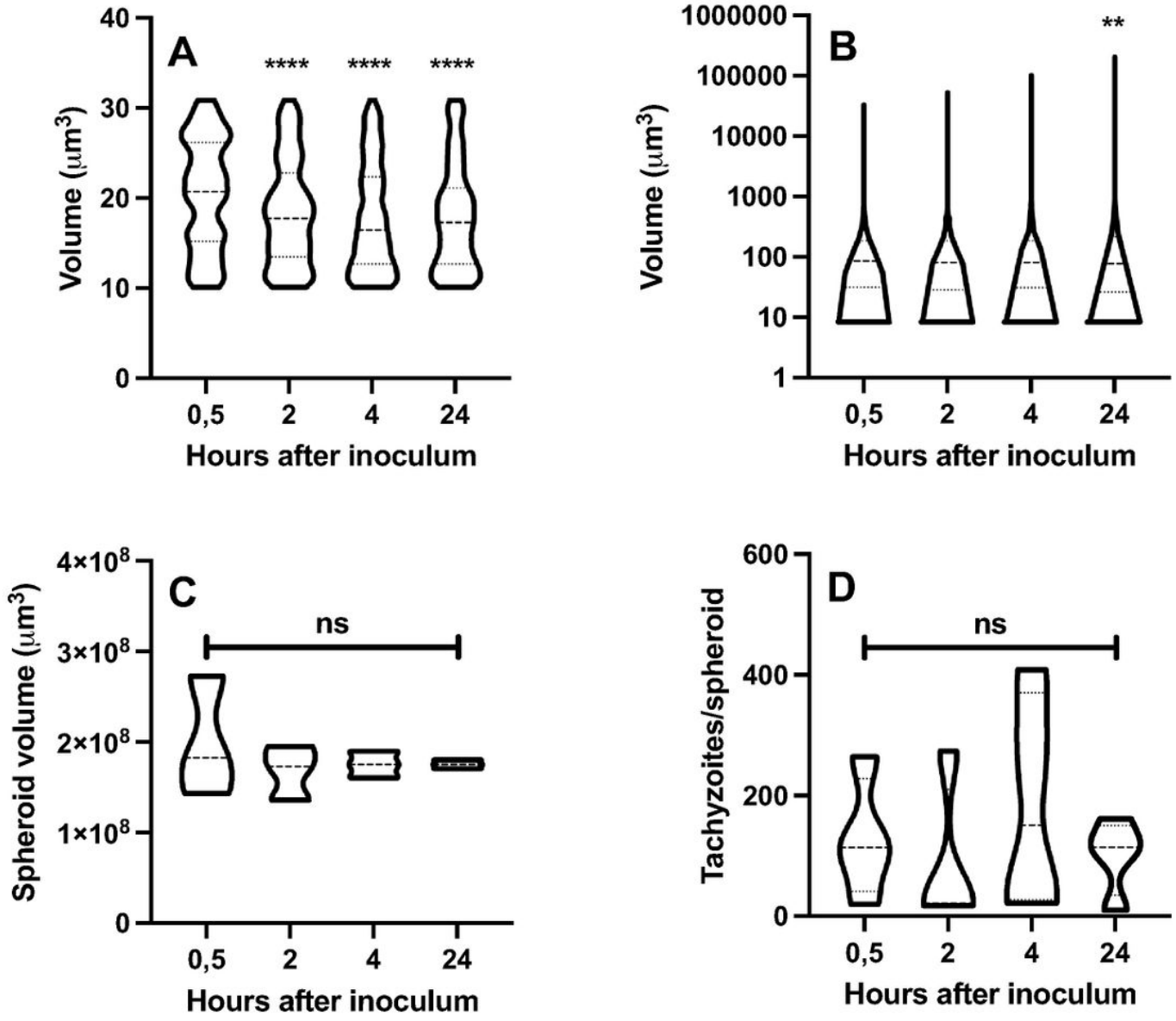

Figure 9

Volumes in µm^3 of *T gondii* tachzoites (A), NIH/3T3 nuclei (B), spheroids (C) and total count of tachyzoites (D) found in spheroids. (****): p< 0.0001. (**): p< 0.01.

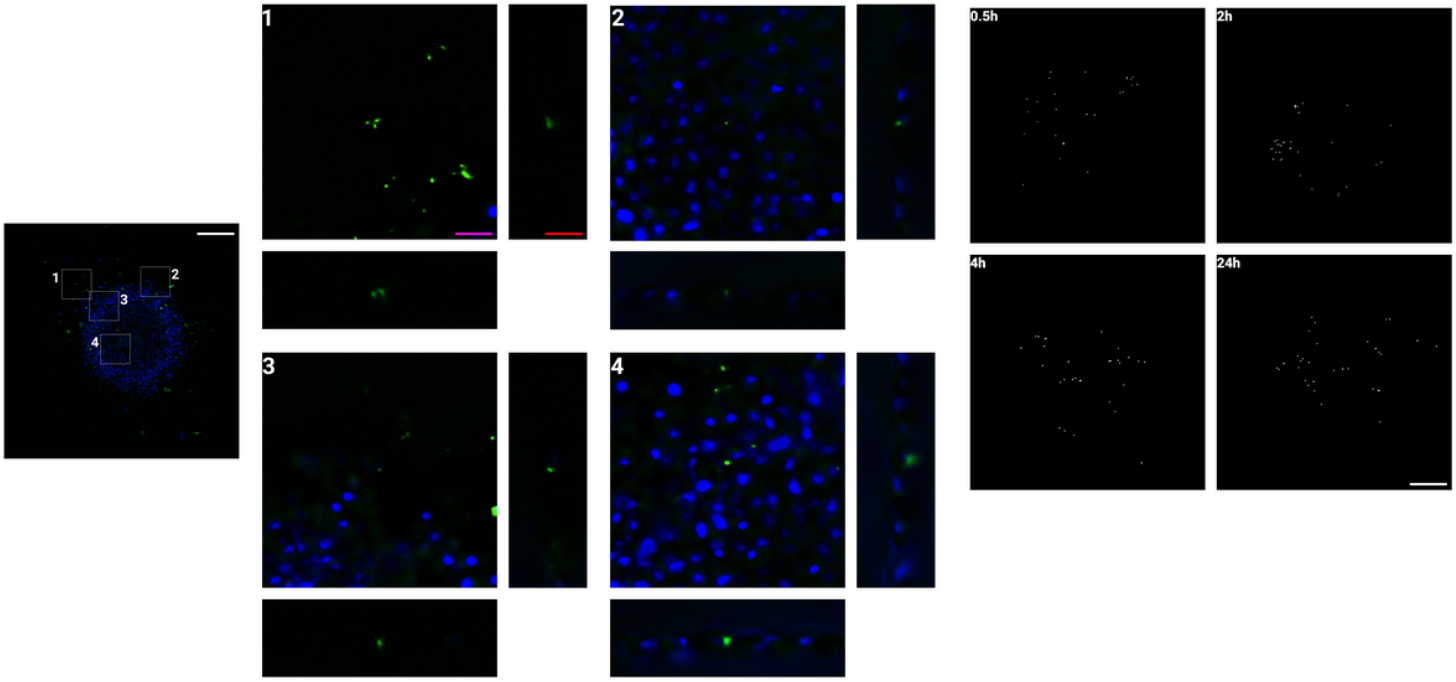

Figure 10

Rhodamine 123-positive events in spheroid 24 hours after infection. Left: Whole spheroid and four highlighted regions of interest containing relevant events. Magnification: 4X. Scale bar (white): 200µm. (1), (2), (3) and (4): Digital zoom (16X) of highlighted regions and its respective orthogonal (YZ and XZ) views. Scale bars: 50µm (magenta) and 5µm (red). Pseudocolored events: blue – NIH/3T3 nuclei (Hoechst 33342); green – *T. gondii* tachyzoites (Rhodamine 123).

Supplementary Files

This is a list of supplementary files associated with this preprint. Click to download.

- suppl.jpg
- supplmat.docx